Supporting Information

Optical Index Prism Sensitivity of Surface Plasmon Resonance Imaging in Gas Phase: Experiment versus Theory

Jonathan S. Weerakkody,[†] Sophie Brenet,[†] Thierry Livache,[‡] Cyril Herrier,[‡] Yanxia Hou,[†] and Arnaud Buhot[*,†]

†*Univ. Grenoble Alpes, CEA, CNRS, IRIG, SyMMES, 17 Rue des Martyrs, 38000 Grenoble, France*

‡*Aryballe Technologies, F-38000 Grenoble, France*

E-mail: arnaud.buhot@cea.fr

Theoretical considerations

A matrix M was used to relate the ratio of the tangential fields for the successive layers. This global transfer matrix M also referred to as the characteristic matrix of the multi-layer structure was obtained by multiplying the intermediate matrices as shown in Equation 1. Where the M_k matrices are derived as a function of the optical and magnetic properties of the $N-$layers, its thicknesses, and the wavelength (λ) and internal angle of incidence (θ_{in})

of the beam of light.

$$M = \prod_{k=2}^{N-1} M_k = \begin{bmatrix} M_{11} & M_{12} \\ M_{21} & M_{22} \end{bmatrix} \tag{1}$$

with

$$M_k = \begin{bmatrix} cos\beta_k & \frac{-\imath sin\beta_k}{q_k} \\ -\imath q_k sin\beta_k & cos\beta_k \end{bmatrix}$$

where

$$q_k = \sqrt{\frac{\mu_k}{\epsilon_k}} \sqrt{\frac{1 - Re\sqrt{[\epsilon_1\mu_1]}^2 sin^2[\theta_{in}]}{\epsilon_k\mu_k}}$$

For, $k \leq N-1$

$$\beta_k = \frac{2\pi d_k}{\lambda} \sqrt{\epsilon_k\mu_k - \epsilon_1\mu_1 sin^2[\theta_{in}]}$$

else, for the semi-infinite first and last layers $\beta_k = 0$.

The reflectivity R, as a percentage, can then be calculated with Equation 2 for $p-$ polarized light in the Transverse Magnetic (TM) mode. Since prisms were used experimentally; an additional transmission function T was introduced .[1] Where the transmission is expressed in terms of prism apex angle (θ_{Ap}), optical index of the prism (n_1) and external incident angle (θ_{ex}). This function returns the attenuation coefficient of the luminous intensity of the incident beam, to account for the transmission losses through the prism faces. Therefore, in this case, θ_{ex} would be used instead of θ_{in} due to refraction considerations.

$$R = 100\left|\frac{(M_{11} + M_{12}q_N)q_1 - (M_{21} + M_{22}q_N)}{(M_{11} + M_{12}q_N)q_1 + (M_{21} + M_{22}q_N)}\right|^2 T[\theta_{Ap}, n_1, \theta_{ex}] \tag{2}$$

where for the first layer,

$$q_1 = \sqrt{\frac{\mu_1}{\epsilon_1}} cos[\theta_{in}]$$

and

$$T[\theta_{Ap}, n_1, \theta_{ex}] = \frac{(2cos[\frac{\pi}{2} - \frac{\theta_{Ap}}{2} - \theta_{ex}])^2 (2n_1 cos[arcsin[\frac{sin[\frac{\pi}{2} - \frac{\theta_{Ap}}{2} - \theta_{ex}]}{n_1}]])^2}{(cos[arcsin[\frac{sin[\frac{\pi}{2} - \frac{\theta_{Ap}}{2} - \theta_{ex}]}{n_1}]] + n_1 cos[\frac{\pi}{2} - \frac{\theta_{Ap}}{2} - \theta_{ex}])^4}$$

and θ_{ex} is expressed as a function of θ_{in}, perpendicular to the surface of the prism;

$$\theta_{ex} = \frac{\pi}{2} - \frac{\theta_{Ap}}{2} - arcsin[n_1 sin[\frac{\pi}{2} - \frac{\theta_{Ap}}{2} - \theta_{in}]]$$

Additional figures

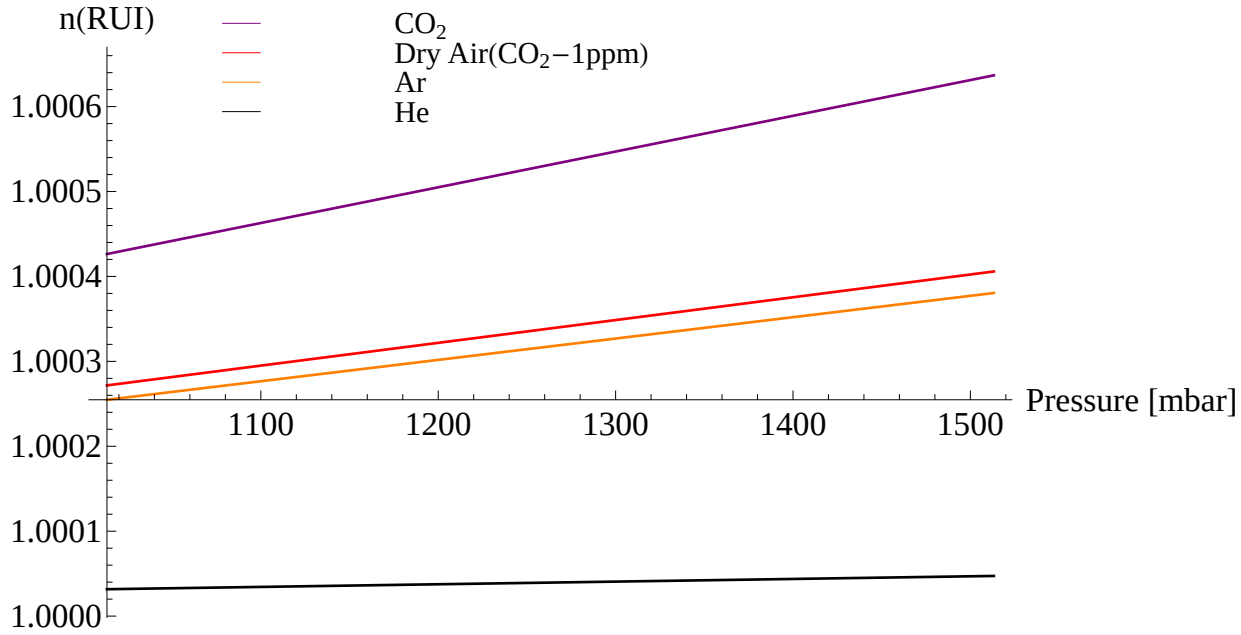

Figure S1: Change in refractive index (n) with respect to the change in pressure for the 4 different gases tested. The relationship for the pure gases were obtained by using the Hauf-Grigull relation .[2] For Dry Air, a more complex, Sellmeier equation based model was used containing dependencies on temperature, pressure, humidity and CO_2 concentration .[3]

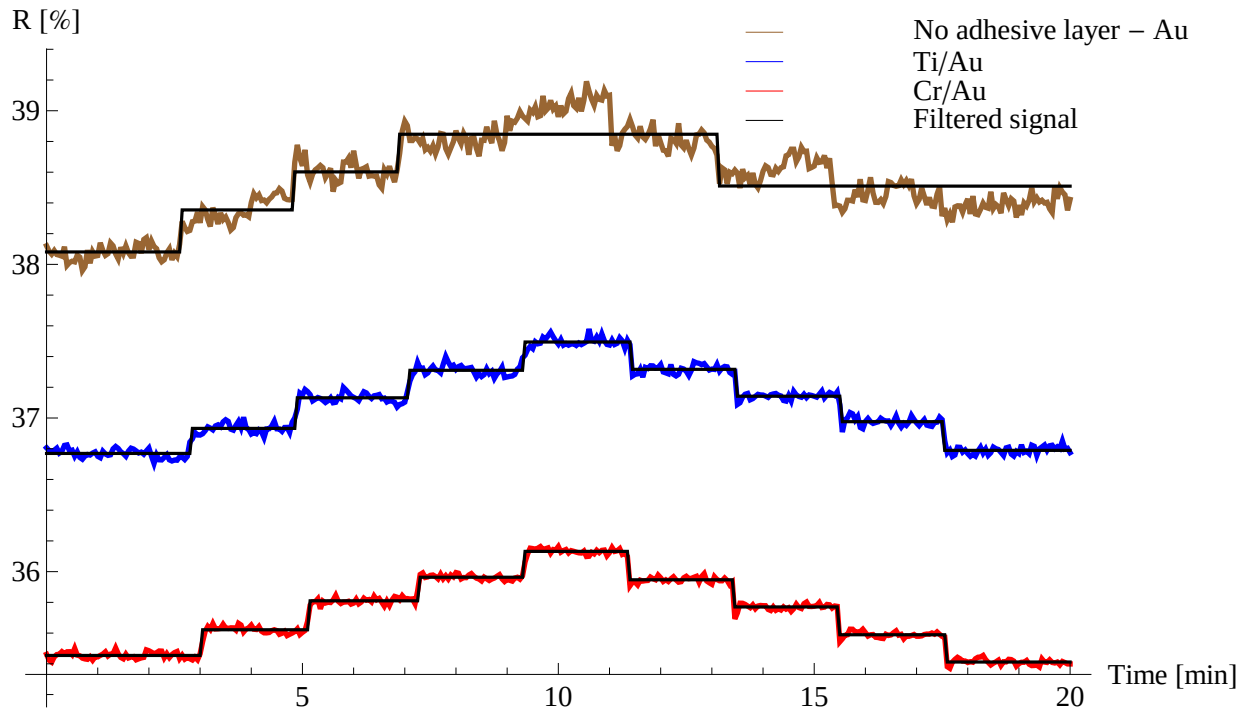

Figure S2: Temporal response of the SPR imaging system for the 3 sample prisms (Cr/Au, Ti/Au, and Au (no adhesive layer)). The graphs represent a single pressure jump experiment averaged over 5 spots; carried out at $25°C$ and with a working angle $\theta_w = 42.5°$. A mean shift filter was used to filter out a noise level of 0.05% and 0.07%, respectively, for Cr/Au sample 1 and Ti/Au sample 2. The noise range of sample 3 with no adhesive layer was $> 0.13\%$, coupled with a high drift, gave a corrected signal unviable for further processing. The noise and drift are seen to decrease with better Au adherence on glass prisms from no adhesive layer to the Cr adhesive layer.

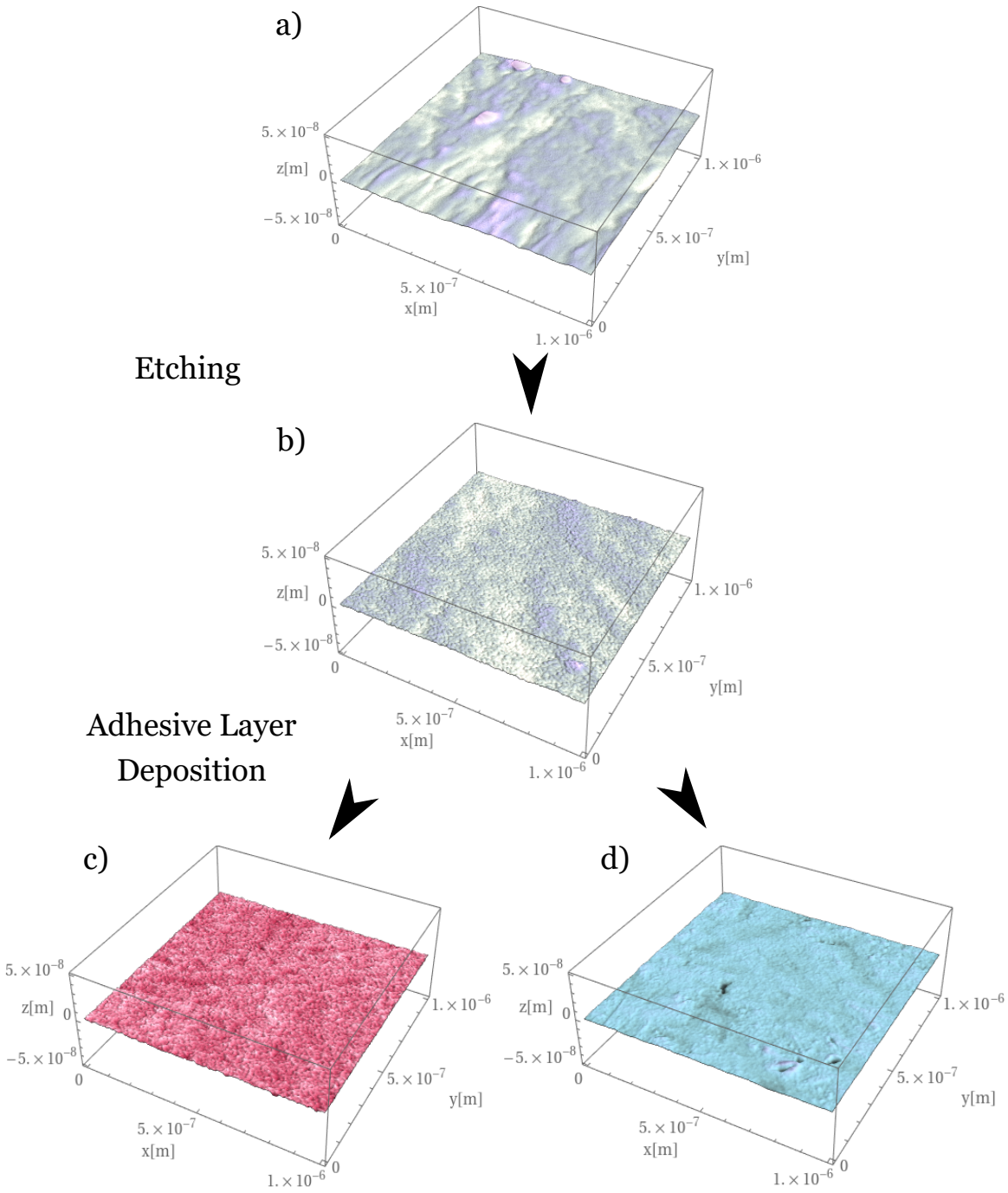

Figure S3: AFM analyses of surface topography for every intermediate steps during SPR imaging prism preparation. No regular grain structures were observed. This shows that the grains observed on sample 1 and 2 were mainly caused by these adhesive layers as a result of the improved surface wetting leading to multiple nucleation regions during Au deposition. a) NBK-7 prism prior to etching or metal thin film deposition, $R_q = 1.06nm$. b) NBK-7 prism after etching process, $R_q = 0.60\,nm$. c) After Cr deposition, $R_q = 0.50\,nm$. d) After Ti deposition, $R_q = 0.45\,nm$.

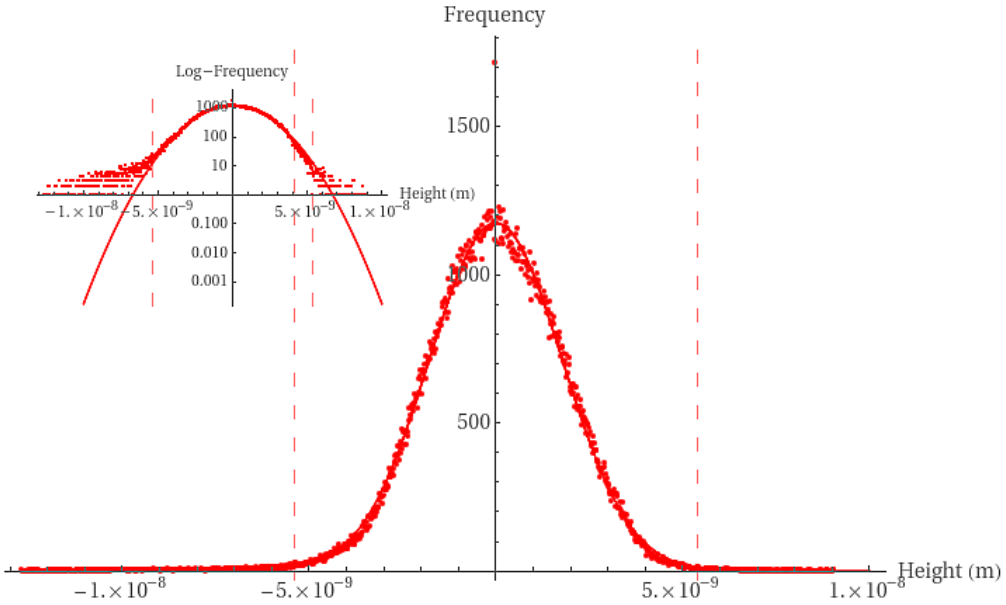

(a) Cr - z-axis Height distribution ($3\sigma = a_z = 5.4\,nm \rightarrow d_{eff} = 10.8\,nm$)

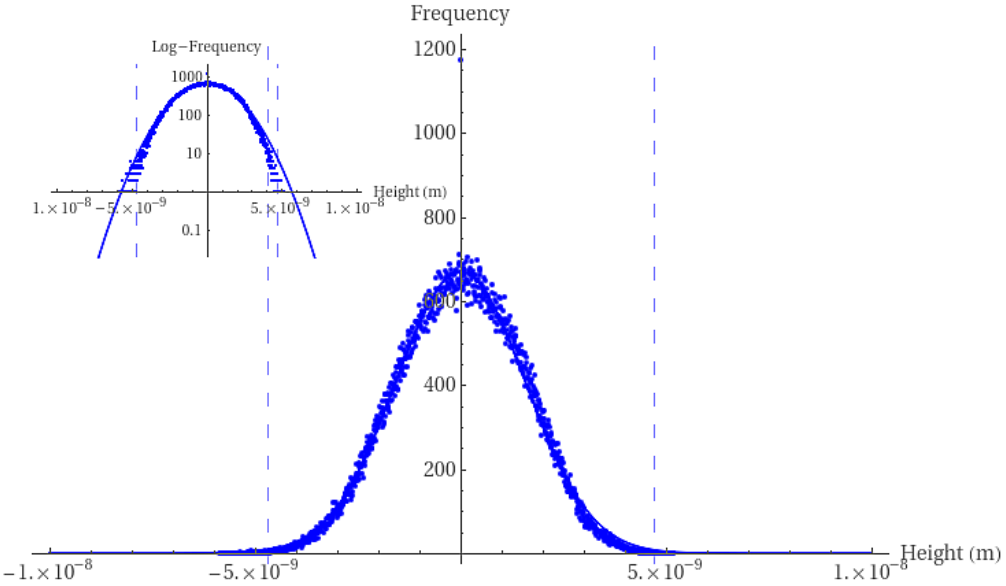

(b) Ti - z-axis Height distribution ($3\sigma = a_z = 4.7\,nm \rightarrow d_{eff} = 9.4\,nm$)

Figure S4: The z-axis heights, from each pixel of the AFM images, was placed into bins (total of 1000 bins) to create a distribution. This allowed for a more accurate estimation of the average grain height. The distribution was fitted with a Gaussian fit; 3σ width is highlighted using dotted lines. **Inset** - The Log scaled-frequency of the distribution to represent the trailing ends of these distributions.

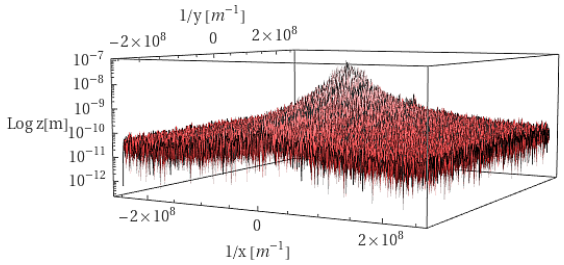

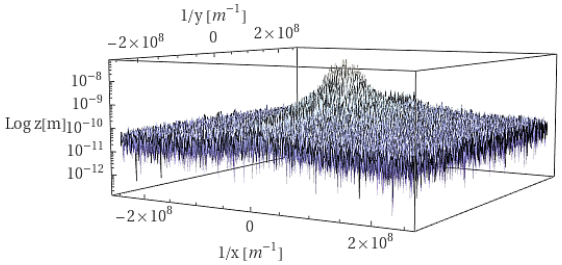

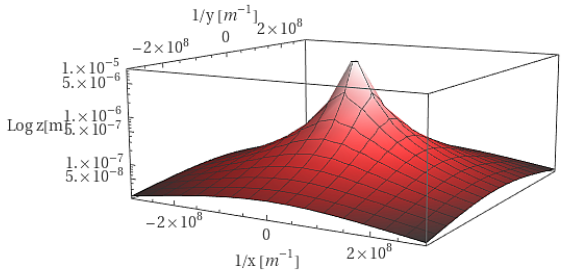

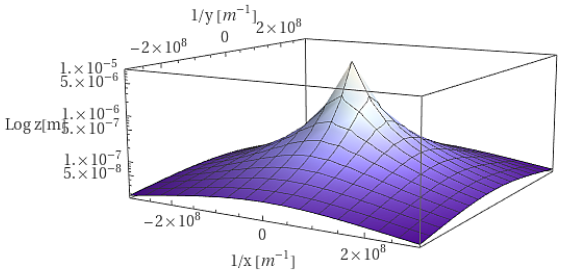

(a) Cr - 2DFFT Lorentzian fit ($a_x = 30.8\,nm$ and $a_y = 29.3\,nm$)

(b) Ti - 2DFFT Lorentzian fit ($a_x = 29.3\,nm$ and $a_y = 27.5\,nm$)

Figure S5: The 2D FFT data for both the a) Cr and b) Ti adhesive layer prism samples were plotted as a 3D plot (top), following the representative Lorentzian fit which was used to obtain a_x and a_y (bottom). Note that plots were Log-scaled to highlight the better fit with Lorentzian compared to its Gaussian counterpart.

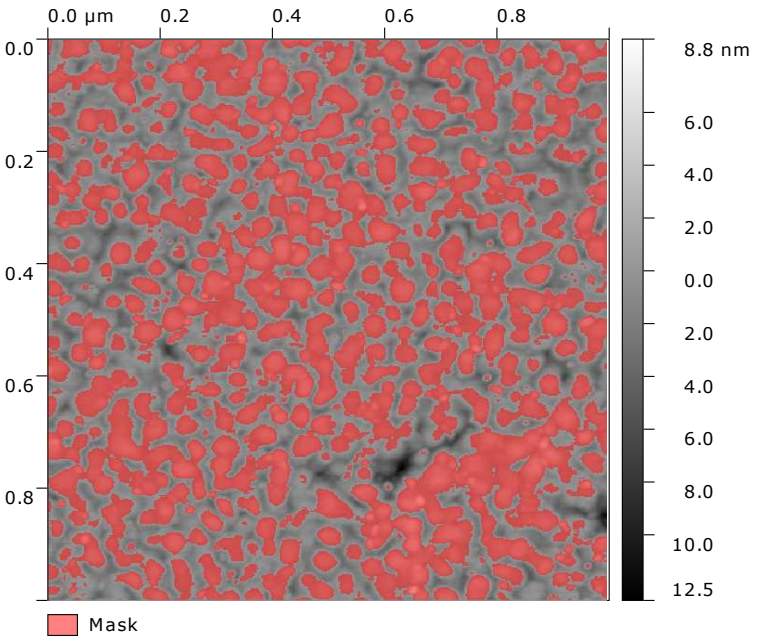

(a) Cr - Total projected area (rel.) - 50.6%

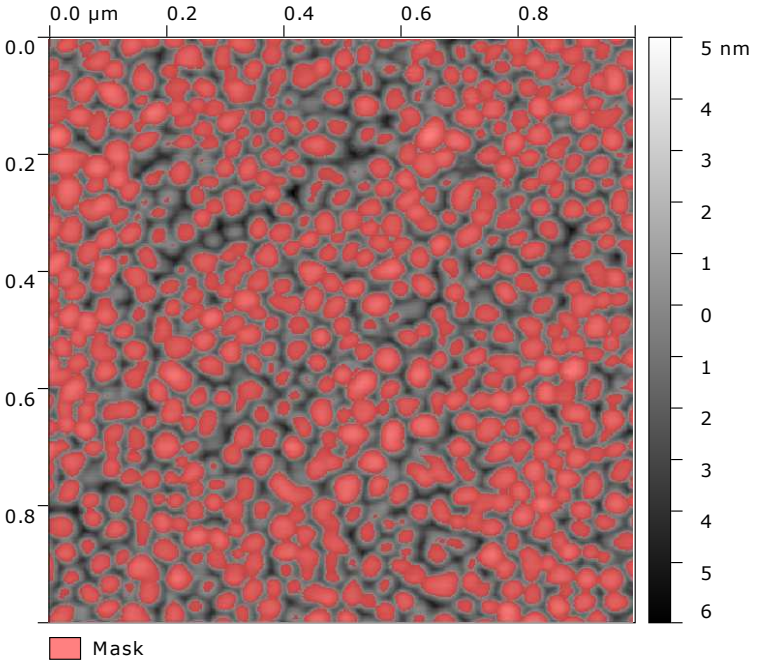

(b) Ti - Total projected area (rel.) - 51.1%

Figure S6: Gwyddions' built-in, automated Otsu's thresholding was used to estimate the surface coverage. For both samples the relative project area of the grains were very similar $\approx 51\%$

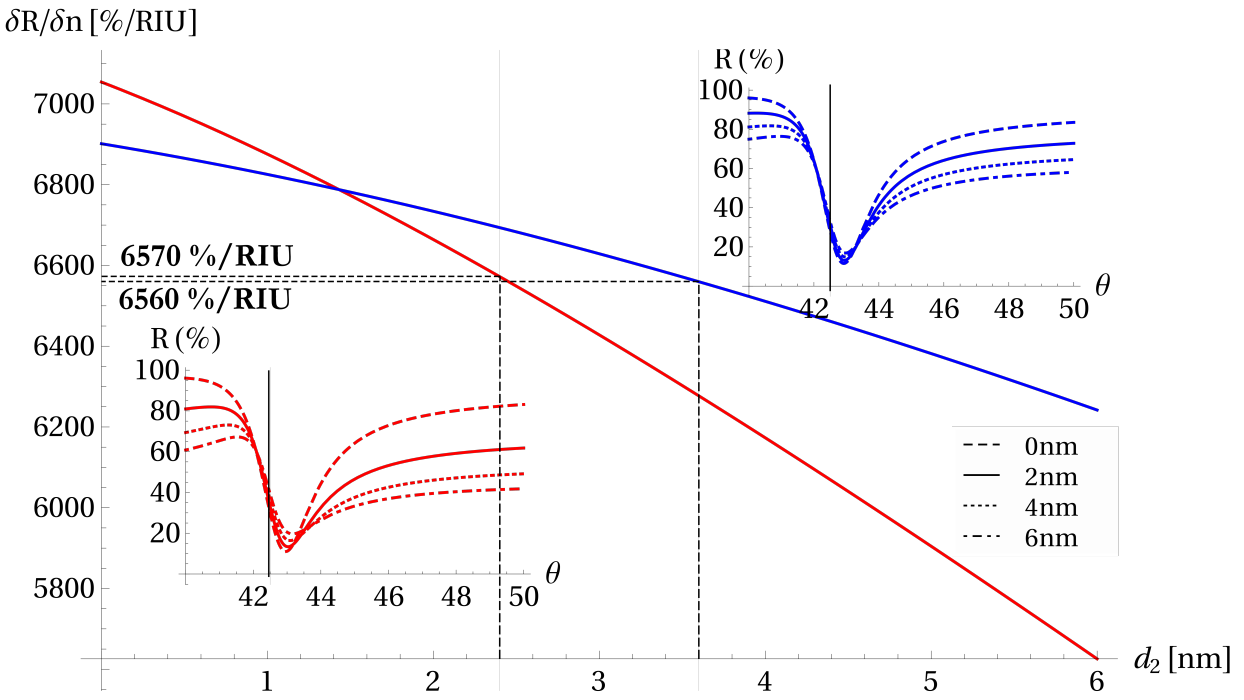

Figure S7: Theoretical $\partial R/\partial n$ for both Cr (Red) and Ti (Blue) with respect to the thickness of each adhesive layer. Results were obtained via the $5-$layer model which includes the effective layer containing the surface topography considerations; the model was established with Au thicknesses generated from the deposition ($54.5\,nm$) and at a fixed working angle of $42.5°$. **Inset(s)** - Reflectivity (%) with respect to the angle (θ) for both Cr (bottom) and Ti (top) at adhesive layer thicknesses $0, 2, 4$, and $6\,nm$.

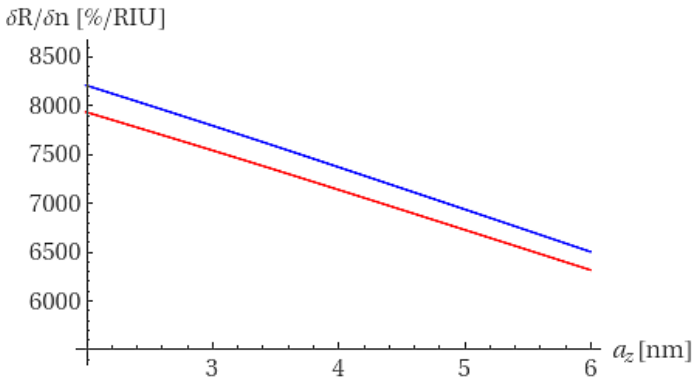

(a) $\partial R/\partial n$ changes with a_z for Cr (red) and Ti (blue). Values for $a_{x,y}$ and f were constrained at $30\,nm$ and 0.5, respectively.

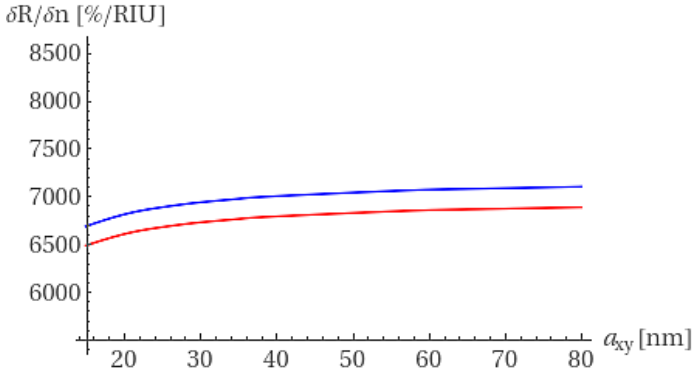

(b) $\partial R/\partial n$ changes with $a_{x,y}$ for Cr (red) and Ti (blue). Values for a_z and f were constrained at $5\,nm$ and 0.5, respectively.

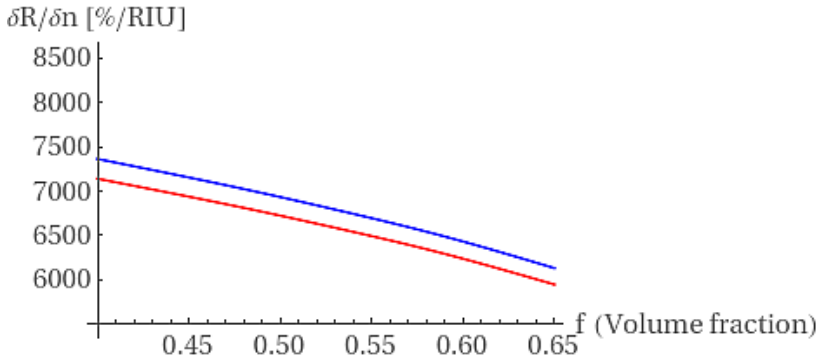

(c) $\partial R/\partial n$ changes with f for Cr (red) and Ti (blue). Values for a_z and $a_{x,y}$ were constrained at $5\,nm$ and $30\,nm$, respectively.

Figure S8: Grain geometry and volume fraction impact on $\partial R/\partial n$. In each case, two of the three parameters were constrained to closely represent experimentally derived values. Followed conditions $a_x = a_y > 3a_z$. The working angle θ_w is set to the angle maximizing the sensitivity θ_{max}.

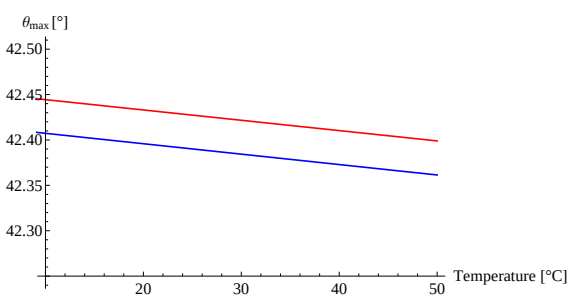

(a) The angle maximizing the sensitivity θ_{max} with respect to the change in temperature for Cr (red) and Ti (blue).

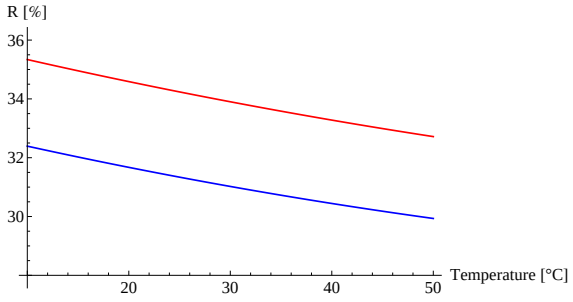

(b) Reflectivity change with temperature at a θ_w set to 42.5° for Cr (red) and Ti (blue). A signal drift of $\approx 0.04\,\%/°C$ was observed.

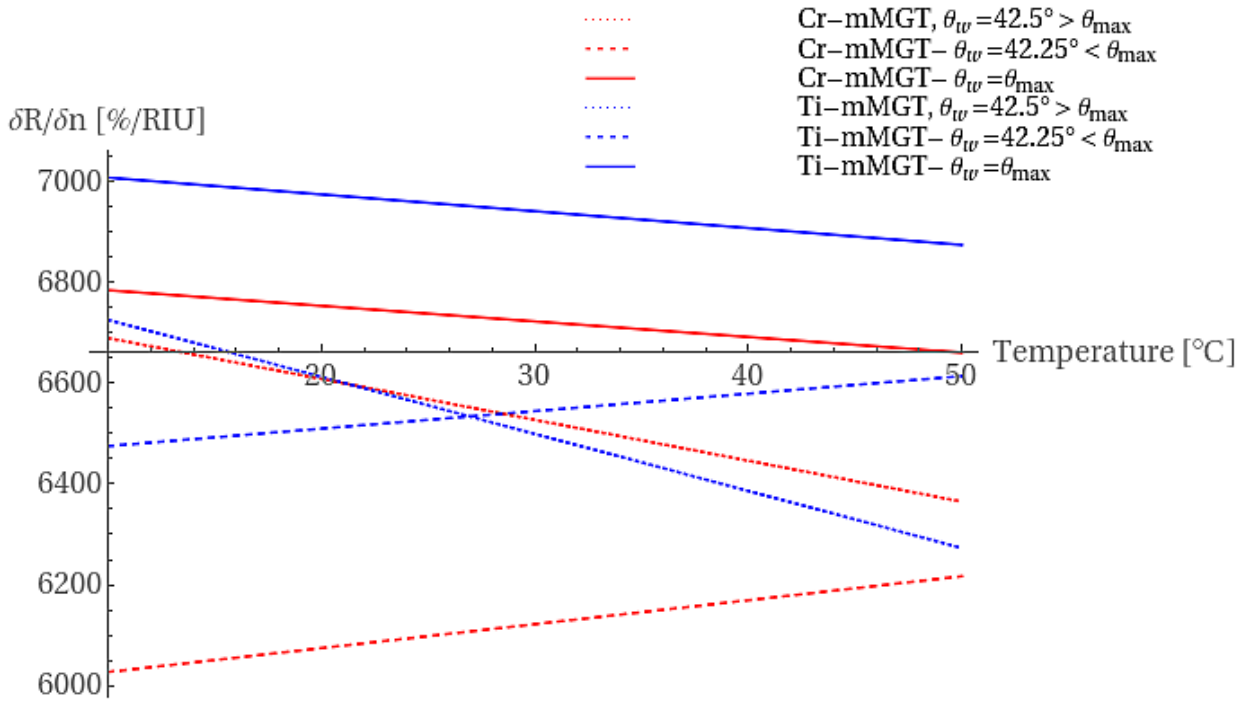

(c) The sensitivity $\partial R/\partial n$ increases with a decrease in temperature for Cr and Ti adhesive layers at $\theta_w > \theta_{max}$. The relationship is inversed when $\theta_w < \theta_{max}$. The sensitivity is optimal for $\theta_{max}(T)$ which is decreasing at a lower rate with increasing temperature.

Figure S9: The effect of temperature change on the reflecivity signal and sensitivity of the SPR imaging prisms and its relationship to the working angle θ_w. Inversion of temperature effects are observed depending on the working angle position with respect to θ_{max}.

References

(1) Laplatine, L.; Leroy, L.; Calemczuk, R.; Baganizi, D.; Marche, P. N.; Roupioz, Y.; Livache, T. Spatial resolution in prism-based surface plasmon resonance microscopy. *Optics Express* **2014**, *22*, 22771.

(2) Sang, B. H.; Jeon, T.-I. Pressure-dependent refractive indices of gases by THz time-domain spectroscopy. *Optics Express* **2016**, *24*, 29040.

(3) Ciddor, P. E. Refractive index of air: new equations for the visible and near infrared. *Applied Optics* **1996**, *35*, 1566.